EPJ E
Soft Matter
www.epj.org

Eur. Phys. J. E **27**, 13–20 (2008) DOI: 10.1140/epje/i2007-10365-2

Anisotropic colloids through non-trivial buckling

C. Quilliet, C. Zoldesi, C. Riera, A. van Blaaderen and A. Imhof

EDP SCIENCES
Società Italiana Di Fisica
Springer

Eur. Phys. J. E **27**, 13–20 (2008)
DOI 10.1140/epje/i2007-10365-2

THE EUROPEAN PHYSICAL JOURNAL E

Anisotropic colloids through non-trivial buckling

C. Quilliet[1,2,a], C. Zoldesi[2], C. Riera[3], A. van Blaaderen[2], and A. Imhof[2]

[1] Laboratoire de Spectrométrie Physique, CNRS UMR 5588 and Université Joseph Fourier, 140 avenue de la Physique, 38402 Saint-Martin d'Hères Cedex, France
[2] Soft Condensed Matter, Debye Institute for Nanomaterials Science, Faculty of Science, Utrecht University, Princetonplein 5, 3584 CC Utrecht, The Netherlands
[3] DEAS, Harvard University, 29, Oxford Street, Cambridge MA 02138, USA

Received 29 March 2007 and Received in final form 27 February 2008
Published online: 1 August 2008 –

Abstract. We present a study on buckling of colloidal particles, including experimental, theoretical and numerical developments. Oil-filled thin shells prepared by emulsion templating show buckling in mixtures of water and ethanol, due to dissolution of the core in the external medium. This leads to conformations with a single depression, either axisymmetric or polygonal depending on the geometrical features of the shells. These conformations could be theoretically and/or numerically reproduced in a model of homogeneous spherical thin shells with bending and stretching elasticity, submitted to an isotropic external pressure.

PACS. 46.32.+x Static buckling and instability – 82.70.Dd Colloids – 89.75.Kd Patterns

1 Introduction

Anisotropic colloidal particles made using spheres have been the subject of various studies in recent years. These types of colloids can be obtained in very different ways, for example either by deformation of spherical particles [1–3], or by forming clusters of them [4–7]. Such objects are good candidates to generate anisotropic colloidal crystals. Photonic bandgap (PBG) calculations showed that such crystals should improve the expected performances (larger bandgap, more convenient wavelengths) [4,8,9]. Colloids with a hollow interior (spherical shells) are particularly interesting also for their mechanical properties, which make them potentially important for a variety of applications, such as drug delivery, catalysis and biotechnology, and when filled with gas as contrast agents for ultrasound or echographic imaging [10,11]. Due to the relevant engineering situations as well as the biomechanics, the problem of the deformation of a spherical shell under external constraints has been recently investigated, both experimentally and numerically [12–18].

In this study, we present anisotropic colloids obtained by buckling of spherical shells. The buckling was induced by dissolving or evaporating the solvent enclosed in the slightly porous shells. This causes a stress comparable to an isotropic pressure on a spherical airproof shell [19]. After postbuckling, the colloidal shells show bowl-like conformations, either with axisymmetric or polygonal symmetry. We observed them using both transmission optical microscopy and transmission electron microscopy (TEM), and compared them with configurations obtained from Surface Evolver simulations, using a model of homogeneous elastic (bending and in-plane stretching) spherical shells submitted to an isotropic external pressure.

[a] e-mail: Catherine.Quilliet@ujf-grenoble.fr

2 Buckling under evaporation and in solution

2.1 Methods

Spherical colloidal shells were prepared following previous work by Zoldesi and co-authors [20,21]. They vigorously mixed dimethyldiethoxysilane (DMDES) and an aqueous solution of ammonia (NH_3), providing a very monodisperse and stable oil-in-water emulsion with droplets of micrometric size. The oil consists of low molecular polydimethylsiloxane (PDMS) oligomers. By adding tetraethoxysilane (TEOS), a solid shell forms at the surface of the droplets, consisting mainly of PDMS with average oligomer length 4, crossed-linked with hydrolyzed TEOS units. As shown in reference [21], the shells are porous and then allow small molecules to pass through. As the low molecular PDMS can be dissolved in ethanol [22], adding ethanol (an equal volume in the present study) to such an aqueous suspension of shells filled with oil, leads to dissolution of the encapsulated oil into the external medium. For thick enough shells ("capsules" and spheres in the nomenclature of ref. [21], *i.e.* shell thickness over 100 nm), this leads to a suspension of solvent-filled spherical particles. These particles are then sedimented

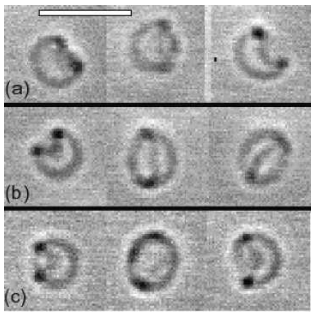

Fig. 1. Typical transmission optical microscopy images of particles from a suspension of colloidal spheres filled with oil, in a mixture of water and ethanol. Three different objects are displayed under three different views; they all show the same coffee-bean buckled shape, with an elongated depression. Scale bar 4 μm.

by centrifugation and redispersed in ethanol. They may be dried afterwards and observed by electron microscopy, exhibiting shape modifications ("buckling under evaporation") or not [20,21], depending on the ratio of their shell thickness to radius [19].

Thinner shells, however, will already buckle in solution when ethanol is added. Thin shells consist of much larger PDMS oil droplets coated with a very thin solid organosilica layer. They were prepared using the same procedure as described in reference [20] for "microballoon" particles. In order to obtain bigger particles, we increased the concentration of DMDES and ammonia up to 5% v/v, and the droplets were allowed to grow for three days before the encapsulation step. This resulted in somewhat more polydisperse particles with diameters between 3 and 6 μm. Since this small polydispersity prevented from determining the shell thickness through static light scattering, we had to use alternative techniques to estimate it. A range of 5–20 nm was proposed [20] by considering that all the TEOS forms a dense silica shell, but careful observations of transmission electronic microscopy (TEM) pictures suggest 10–40 nm, which is likely since PDMS oligomers are known to co-polymerize with TEOS, hence contributing to the shell thickness.

2.2 Experimental results

In order to resolve the post-buckling structure by transmission optical microscopy, we used batches of larger particles with radii R between 2 and 3 μm. Once buckled in solution through addition of ethanol as described in the previous section, these particles hold a single depression with significant volume compared to that of the initial sphere. Furthermore, in some cases the depression is not axisymmetric anymore. In one batch (Fig. 1), we did observe apparently identical objects, all with an elongated depression that gives the whole object a coffee-bean shape. This type of conformations was reported in the literature for red blood cells [23] and for polystyrene shells previously filled with organic compounds and evaporated in air [24,25], and was reproduced by numerical simulations [26].

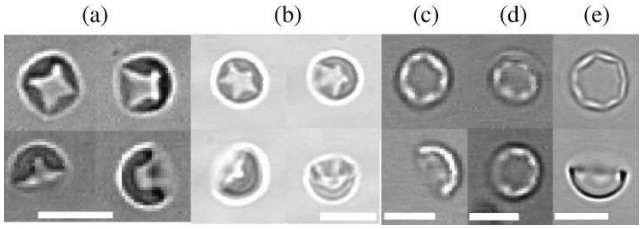

Fig. 2. Spherical shells buckled in solution, showing 4 to 8 wrinkles (a-e). Each sub-figure shows different transmission optical microscopy views of the same object. Scale bar 5 μm, except sub-figure (c): 2 μm.

In other cases, the depression presented a polygonal aspect due to regularly spaced radial wrinkles, in a number varying from 4 to at least 8 (Fig. 2), 7–8 being the upper limit that we could still distinguish and count for these shell sizes with optical microscopy.

The obtainment of such structures in solution from synthetic colloids is a total novelty. Besides, shapes with a depression presenting a 3-fold symmetry were previously observed in red blood cells [23,26,24] or in dried polymer particles [24,25] but we could not find in the literature observations concerning a higher number of wrinkles, on any system. To our knowledge, theoretical predictions leading to such wrinkles do not exist either, except when generated by a point [27,28] or a flat [29] load, which is not the case here.

It is interesting to find out whether some shell heterogeneity has to be invoked to explain such a non-symmetry, or if a model of elastic homogeneous spherical shells is sufficient to recover these non-trivial shapes. For this purpose, we are interested in a model of thin spherical shells with bending and 2D stretch elasticity, that we derived both analytically and numerically. Such an approach was likely to give hints on features hardly accessible by experiments, such as, here, shell thickness, or the successive steps that lead to the final (and observable) shape adopted by the shells.

3 Theoretical part: thin plate elasticity

The elastic energy stored in the deformation of a thin sheet of an isotropic and homogeneous material may be split into a bending and a stretching part [30], and both can be written in terms of surface elasticity:

$$F = \int_{\text{shell surface}} \left(\frac{1}{2}\kappa \left(c - c_0\right)^2 + \frac{1}{2}\epsilon_{ij} K_{ijkl} \epsilon_{kl} \right) \mathrm{d}S, \quad (1)$$

where κ is the bending constant, c_0 the spontaneous curvature of the shell (which is zero for an unstress flat sheet, but $1/R$ for a spherical shell without constraints) [31], and ϵ_{ij} and K_{ijkl}, respectively, the two-dimensional strain and elasticity tensors. The non-zero terms of the two-dimensional elasticity tensor are $K_{xxxx} = K_{yyyy} = \frac{A}{1-\nu^2}$, $K_{xxyy} = K_{yyxx} = \frac{\nu A}{1-\nu^2}$ and $K_{xyxy} = K_{yxyx} = \frac{A}{1+\nu}$

(with A the equivalent two-dimensional Young modulus and ν the equivalent two-dimensional Poisson ratio) [33]. The stretch elasticity term can thus be rewritten as $\frac{A}{2(1+\nu)}[\mathrm{Tr}(\epsilon^2) + \frac{\nu(\mathrm{Tr}\,\epsilon)^2}{1-\nu}]$. We ignored the Gaussian curvature term [32] since, according to the Gauss-Bonnet theorem, its integral depends only on the topology for a closed surface.

To establish the link between these two-dimensional elastic parameters and the three-dimensional features (sheet thickness d, Young modulus E and Poisson ratio σ of the bulk material), we follow Landau's approach [33]. As concerns bending, the distribution of stress in a thin plate under flexion at equilibrium leads to

$$\kappa = \frac{Ed^3}{12(1-\sigma^2)}\,. \tag{2}$$

The 2D Young's modulus A was not taken equal to Ed because this would correspond to a "planar" deformation in Landau's terminology, *i.e.* a deformation of plates at constant thickness, which seems not adequate here. The homogeneous "longitudinal" deformation, *i.e.* without constraints in the perpendicular direction, is indeed more adapted to what happens in the shells. This leads to

$$A = \frac{1+2\sigma}{(1+\sigma)^2}Ed,$$
$$\nu = \frac{\sigma}{1+\sigma}\,.$$

It is worthwhile to notice that, as the three-dimensional Poisson ratio σ has a maximum value of 0.5 (incompressible materials), the two-dimensional Poisson ratio ν of such free plates cannot exceed 1/3. This point was neglected in previous work [34], and can become of some importance if one wants to make a link between the parameters chosen for simulation and the geometrical properties of the shells.

As the surface integral scales like R^2, the dimensionless Föppl-von Karman number $\gamma = \frac{AR^2}{\kappa}$ is likely to drive the succession of configurations resulting from the balance between bending and stretching. In this model of thin shell of elastic isotropic material, we then expect

$$\gamma = 12\left(1-\frac{2\sigma^2}{1+\sigma}\right)\left(\frac{R}{d}\right)^2 = 12\left(1-\frac{2\nu^2}{1-\nu}\right)\left(\frac{R}{d}\right)^2. \tag{3}$$

It is interesting to note that this model predicts conformations to be independent of E, and to finally depend only on the relative thickness d/R and the Poisson ratio.

In such a model, we can calculate the elastic energy of an initially unstrained spherical surface whose inner volume decreases by ΔV its initial value V, in two conformations: when the sphere remains spherical, and following reference [35] when an axisymmetric depression is created by inverting a spherical cap:

$$U_{\mathrm{sphere}} = 4\pi R^2 \times \frac{A}{9(1-\nu)}\left(\frac{\Delta V}{V}\right)^2, \tag{4}$$

$$U_{\mathrm{axisym}} = \pi\,\frac{AR^2}{\gamma}\left(\frac{d}{R}\right)^{-\frac{1}{2}}$$
$$\times\left[\sin\alpha\left(\tan\alpha-\left(\frac{d}{R}\right)^{1/2}\right)^2+4\left(\frac{d}{R}\right)^{1/2}(1-\cos\alpha)\right], \tag{5}$$

where $\frac{d}{R}$ can be expressed as a function of γ and ν through equation (3). The parameter α is the half-angle of the revolution cone apexed at the sphere center, and in which the axisymmetric depression inscribes. This half-angle relates to the relative volume variation through

$$\frac{\Delta V}{V} = \frac{1}{2}(1-\cos\alpha)^2(2+\cos\alpha). \tag{6}$$

In the limit of very thin shells and small volume variations, one can show that

$$U_{\mathrm{axisym}} \approx \frac{\pi}{12^{1/4}}AR^2\gamma^{-\frac{3}{4}}\left[1-\frac{2\nu^2}{1-\nu}\right]^{-\frac{1}{4}}\alpha^3.$$

Or, as a function of the relative volume variation

$$U_{\mathrm{axisym}} \approx \frac{4}{3}\frac{\pi}{2^{1/4}}AR^2\gamma^{-\frac{3}{4}}\left[1-\frac{2\nu^2}{1-\nu}\right]^{-\frac{1}{4}}\left(\frac{\Delta V}{V}\right)^{3/4}.$$

In this limit, $U_{\mathrm{sphere}} = U_{\mathrm{axisym}}$ would then happen for relative volume variations

$$\frac{\Delta V}{V} \propto \gamma^{-\frac{3}{5}}\,, \tag{7}$$

which provides a scaling law for the "sphere towards capsule" buckling.

These theoretical calculations will be compared to simulation results in Section 4.4.

4 Simulations

4.1 Modus operandi

The simulated configurations presented hereafter were obtained using the free software Surface Evolver [36], in which the elastic energy given by equation (1) is minimized in the space of conformations. The stretch energy term is in fact calculated using the Cauchy-Green strain tensor, which is accurate for describing deformations of larger amplitude. The minimization was performed by alternating gradient, conjugate gradient and Hessian methods. Stochasticity was introduced by jiggling the position of the vertices at the beginning of each minimization (*i.e.* at each volume step when the volume is decreased by steps). We tested that the number of vertices is high enough to avoid an influence of the mesh on the conformations. Furthermore, we checked that the symmetry of

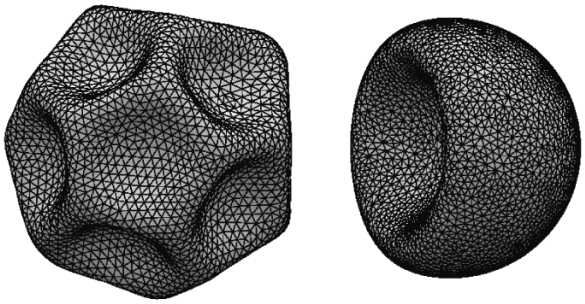

Fig. 3. Conformations numerically obtained with Surface Evolver for $\gamma = 743$, $\nu = 0.333$ (which corresponds to a shell of relative thickness $d/R = 0.116$ of an incompressible material with $\sigma = 0.5$), $\frac{\Delta V}{V} = 0.171$, $c_0 = 1/R$, 3594 vertices. Left: simulation performed by directly minimizing at $c_0 = 1/R$ for each decreasing volume step: $N = 17$ depressions. Right: simulation performed first with $c_0 = 0$, then $c_0 = 1/R$. The elastic energy is 3.10 times larger for the "potato" (left) than for the capsule (right).

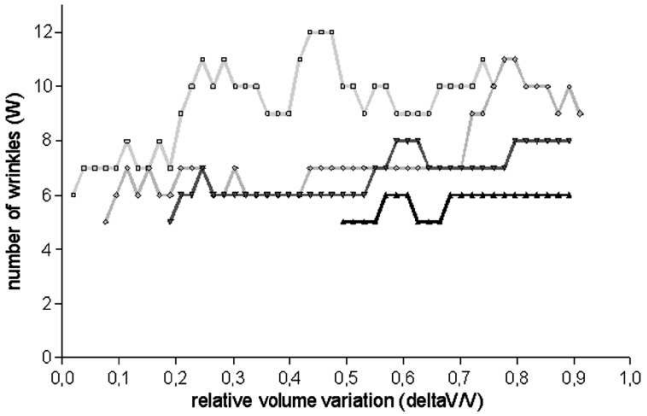

Fig. 4. Typical evolution of the number W of wrinkles held by the single depression after secondary buckling (simulations performed for $\gamma = 2333$ (black, upward pointing triangles), 7465 (dark grey, downward pointing triangles), 15163 (medium grey, diamonds) and 29160 (light grey, squares); $\nu = 0.333$).

the mesh has no influence on the position of the wrinkles, by using an isotropic randomized mesh. Such an approach was initiated by Tsapis *et al.* [34].

We explored a discrete range of γ, and restricted our simulations to the case of an incompressible material, *i.e.* $\nu = 1/3$ ($\sigma = 1/2$).

Given these elastic parameters, a first set of minimization was performed through stepwise decrease of the inner volume of an initially spherical surface, and stress free (*i.e.*, $c_0 = 1/R$), with a minimization at each volume step. This leads to roughly isotropic structures with depressions regularly spaced on the surface, such as in reference [34] or in Figure 3, left. The number of depressions is found to increase with γ.

Different shapes of much lower energy (for the same elastic parameters) could be obtained through more sophisticated minimizations. This was done by reversibly acting on the spontaneous curvature c_0 of the shells. Since the shells are formed by templating on the oil droplets, one can assume that they are unstrained in their initial state and c_0 is expected to be $c_0 = 1/R$. But when c_0 is changed to zero, conformations qualitatively different could be reached: one obtains "capsules" with a single axisymmetric depression. Minimizing again with c_0 back to $1/R$ preserves this capsule conformation, with an energy lower than the potato shape, as exemplified in Figure 3, right. Temporarily imposing a zero spontaneous curvature is likely to lower the energy barrier for the merging of two different depressions at the surface of the sphere, since merging happens through flattening of the high positive curvature ridge that separates the two depressions. This trick apparently helps to get out of some local minima in which the simulated conformations are easily quenched, as is quite usual in buckling problems.

In the following, such a zero-curvature cycle was systematically performed at each volume step, in order to facilitate conformation changes.

4.2 Results

We performed simulations of an elastic closed surface, initially spherical and unstrained, whose inner volume is decreased by volume steps $\mathrm{d}V = 0.0190 \times V_0$, V_0 being the volume of the initial sphere. In all the experiments, V_0 and κ were kept unchanged and γ was varied from 271 to 29160 by changing A.

Simulations are stopped when the surface interpenetrates, which happens for inner volumes of the order 7–11% the initial volume V_0.

Up to $\gamma = 583$, the volume decrease causes a buckling toward the "capsule" conformation, *i.e.* with a single axisymmetric depression, until the surface interpenetrates.

From $\gamma = 933$, axisymmetric capsules undergo a second transition when the volume goes on decreasing, toward a non-axisymmetric conformation. The onset of this second transition is harder to detect since the depression, except for the highest values of γ, only slowly evolves toward a polygonal shape, and then the corners of the polygon turn into wrinkles (limits of the depression concave between the apices). Quantitative data concerning buckling thresholds will nevertheless be given in Section 4.4. We could this way obtain such wrinkled bowls with 5 wrinkles or more. Some trials with re-increasing volume from a wrinkled state also provided conformations with 3 and 4 wrinkles.

More quantitatively, Figure 4 provides the number W of wrinkles observed throughout a stepwise volume decrease for simulations with different γ values. One can notice that there is some fluctuation on W, of one, or even two, units. In fact, performing decreasing-volume simulations with the same parameters does not always lead to the same number of wrinkles. We could get in these situations an order of magnitude for the energy difference between two close conformation (*i.e.* $W = \pm 1$): it can be as small as a few tenths of percent. The energy of a conformation is not strictly determining its occurence: the path followed in the space of conformations has some importance. This

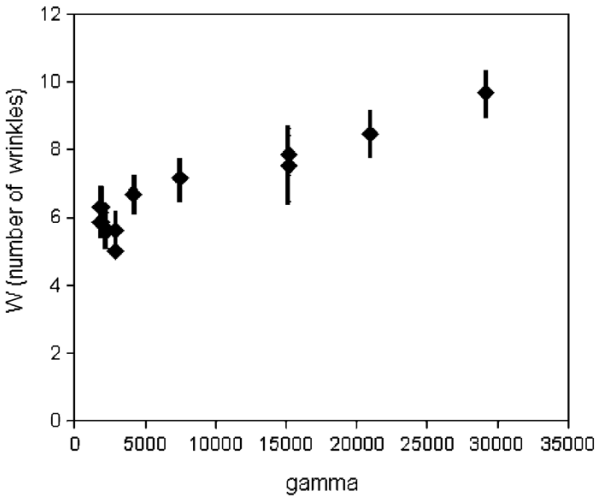

Fig. 5. Number W of wrinkles held by the single depression after secondary buckling, averaged between $\frac{\Delta V}{V} = 0.53$ and $\frac{\Delta V}{V} = 0.76$ (error bar is the standard deviation), as a function of the dimensionless Föppl-von Karman number $\gamma = \frac{AR^2}{\kappa}$.

is why we restricted most of our study to a sequence of minimization that is likely to reproduce the experimental situation, *i.e.* decreasing the volume step by step.

Figure 4 shows a weak tendency for the number of wrinkles W to increase with the relative volume variation $\frac{\Delta V}{V}$ once the buckling has occured, in the same way that was observed in macroscopic indentation experiments [28].

More obvious is the variation of W with γ. In order to precise a variation of a few units on a discrete quantity, we averaged W on a range of $\frac{\Delta V}{V}$ where the conformation holds wrinkles for all the values of γ, *i.e.* $\frac{\Delta V}{V}$ between 0.53 and 0.76 (Fig. 5). This puts into evidence an increase of W with increasing γ. Wrinkles being more numerous with decreasing $\frac{d}{R}$ goes in the sense of intuition: a thinner plate folds more easily, and hence makes more folding patterns.

4.3 Comparison between simulations and experiments

The inner volume of the conformations shown in Figure 2 is not easy to determine precisely. Nevertheless, an important experimental observation is that buckling deformations never relaxed back toward the initial spherical shape after complete evaporation or complete dissolution of the inner oil, yet it means that the last water/air or oil/water interfaces, that were pulling the shell inwards, have disappeared. It is then likely that the shrinking brings opposite surfaces close enough to one another to be sensitive to van der Waals attraction, which would stabilize the buckled conformation against elastic shape recovery after vanishing of the capillary forces. This hypothesis, of initially opposite parts of the shells that contact in the conformations experimentally obtained, seems to be confirmed by confocal pictures of buckled shells (Fig. 6).

In order to compare the shapes obtained through simulations (with decreasing volume) with the experimental

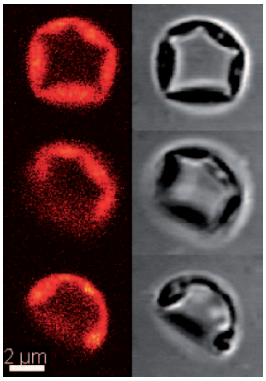

Fig. 6. Three different views of a buckled spherical shell labelled with RITC, in confocal fluorescence microscopy (left) and in transmission microscopy (right). The shell is clearly self-contacting at its convexe part.

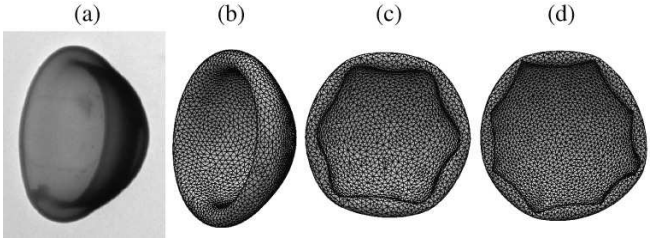

Fig. 7. (a) Capsule obtained from evaporation in air of a spherical shell of mean radius 870 nm, shell thickness 150 nm (TEM image). (b) Simulation obtained for $\gamma = 271$ and $\nu = 0.333$ (hence equivalent to $\frac{d}{R} = 0.172$), $\frac{\Delta V}{V} = 0.854$, 3594 vertices. (c) Simulation: $\gamma = 2333$ and $\nu = 0.333$ (equivalent to $\frac{d}{R} = 0.0586$), $\frac{\Delta V}{V} = 0.854$, 3594 vertices. This conformation is to be compared with Figure 2c. (d) Simulation: $\gamma = 20995$ and $\nu = 0.333$ (equivalent to $\frac{d}{R} = 0.0195$), $\frac{\Delta V}{V} = 0.854$, 3594 vertices. This conformation is to be compared with Figure 2a.

ones, we thus focused on the shapes obtained just before self-contact.

Figures 7a and b show that we could accurately reproduce the shape of axisymmetric capsules. In the simulation displayed here, we took $\gamma = 271$ and $\nu = 0.333$, which corresponds to $d/R = 0.172$.

For wrinkled bowls (examples displayed in Figs. 7c and d), the conformations obtained just before interpenetration are also very similar to shapes observed experimentally (Figs. 2c and e). Like in the experiments, wrinkles do appear for thinner shells. Furthermore, the parameters for which simulations provide wrinkles are consistent with the shells' characteristics: $\sqrt{\frac{12}{\gamma}(1 - \frac{2\nu^2}{1-\nu})} = 0.02$ to 0.08, to be compared to the experimental value $\frac{d}{R} = 0.003$ to 0.04.

Other experimental structures could also be reproduced by simulations, such as the one displayed in Figure 8a. This latter was obtained through evaporation in air of a shell still containing some of its inner oil (note that in this case the ethanol was added in the aqueous solution later than usual, which possibly allowed polymerization of longer chains [21] that cannot be dissolved

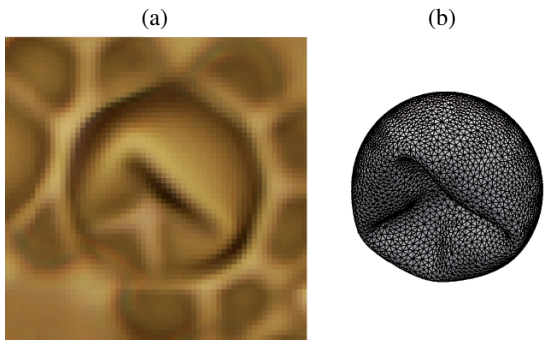

Fig. 8. (a) Shell enclosing oil, evaporated in air ($d/R \approx 0.012$). Transmission optical microscopy, size 17 μm $\times$ μm. (b) Simulation obtained for $\gamma = 2916$ and $\nu = 0.333$ (equivalent to $\frac{d}{R} = 0.064$), by increasing the volume from $\frac{\Delta V}{V} = 0.474$ to $\frac{\Delta V}{V} = 0.209$, 3659 vertices.

by ethanol [37]). Here the inner volume obviously does not correspond to shell self-contact. In such a process, a shrinkage of the shell itself when the water has fully evaporated can be invoked to explain a behaviour comparable to a volume increase, such as in the simulation of Figure 8. The conformation, in this case, is stabilized by oil-air interfaces.

All these results show that there is no need to invoke shell heterogeneity to explain the shapes experimentally observed: bending and in-plane stretching elasticity suffices. The next section provides more quantitative insights on the simulation of elastic buckling.

4.4 Quantitative comparison between simulations and elastic theoretical calculations

The software Surface Evolver used to perform simulations provides the elastic energy of each conformation. For the two conformations "sphere" and "axisymmetric depression", we compared this elastic energy with the theoretical expressions U_{sphere} (Eq. (4)) and U_{axisym} (Eqs. (5) and (6)). The numerical data are very well fitted by the theory, as shown in Figure 9. One sees that this first buckling from a spherical shape to a conformation with a single axisymmetric depression occurs with some hysteresis, *i.e.* for volume variations higher than the one corresponding to $U_{\text{sphere}} = U_{\text{axisym}}$.

Figure 10 presents the buckling occurences as a function of γ. The first buckling is determined without ambiguity, as it is obvious from Figure 9. The occurrence of the second buckling, from an axisymmetric capsule to a "wrinkled bowl" conformation, is less easy to detect since it corresponds neither to a discontinuity nor a singularity in energy. We detected in fact two caracteristic values for $\frac{\Delta V}{V}$, by visual observation of the conformations: the first one corresponds to the loss of the axisymmetry, when the rim of the depression becomes polygonal. Then the apices of the polygon becomes sharper (they tend to form the extremity of a d-cone [28,38]), and the inner part of the rim becomes convex between two successive apices: at this

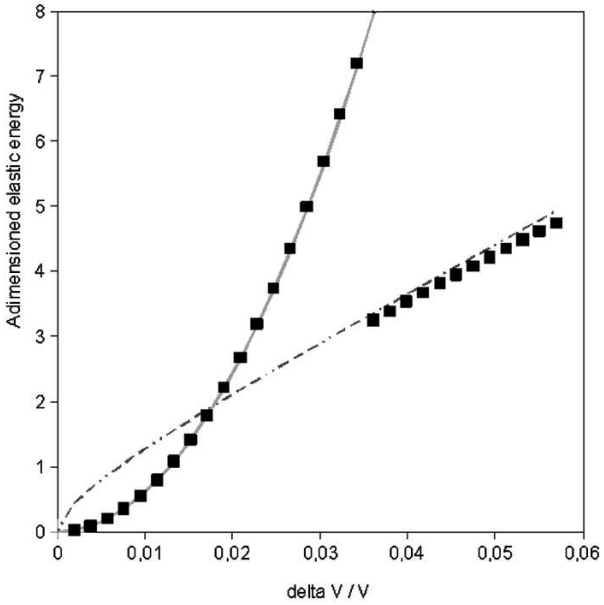

Fig. 9. Elastic energy, adimensioned by κ, of a shrinking shell initially unstrained ($c_0 = 1/R$). Black squares: result of Surface Evolver simulations, with $\gamma = 2916$ and $\nu = 0.333$. Continuous line: normalized elastic energy $U_{\text{sphere}}/\kappa = \gamma U_{\text{sphere}}/(AR^2)$ of a shrinking spherical shell, calculated with same γ and ν according to equation (4). Dot-dashed line: adimensioned elastic energy U_{axisym}/κ of a capsule (deformation with a single axisymmetric depression), calculated with same γ and ν according to equations (5) and (6).

point we consider that the conformation holds wrinkles, and this second "threshold" is recorded. Figure 10 shows that both values are quite close and present the same power law in γ^{-1}. Extrapolation intercepts with $\frac{\Delta V}{V} = 1$ at a value $\gamma_c = 850$, which is consistent with our simulations showing that secondary buckling appears for γ between 583 and 933 ($\frac{d}{R} \approx 0.1$). This can be compared with calculations of reference [27] that forecast a threshold γ of 1345 for the apparition of wrinkles on a clamped cap submitted to concentrated load.

The first buckling (sphere toward axisymmetric capsule) happens for thresholds values of the relative volume variation that vary in a power law with the Föppl-von Karman parameter: $\frac{\Delta V}{V} \propto \gamma^{-0.55}$. Despite the slight hysteresis in the primary buckling, this exponent is very close to the -0.6 theoretically proposed in equation (7).

5 Discussion

Experimental and numerical results showed that wrinkled bowls are preferentially observed when a very thin spherical shell lowers its volume. This conformation is quite different from the structures (typically discocytes or stomatocytes) usually obtained for vesicles, where the in-plane elasticity is liquid-like (related parameter: 2D compressibility) [39]. Wrinkles evidences the 2D solid nature of the shells, since it is needed to accommodate the surface of

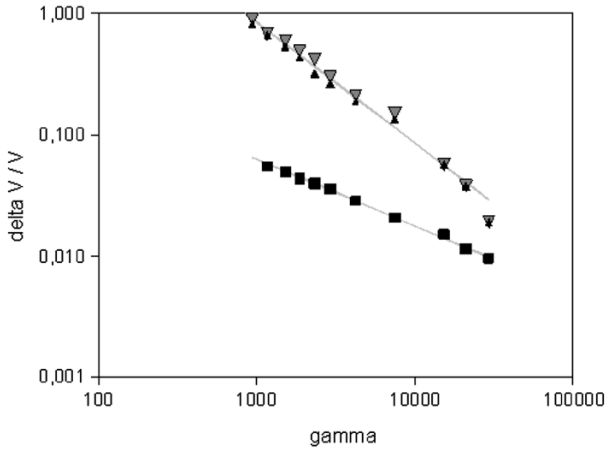

Fig. 10. Primary buckling (black squares) from sphere to capsule: relative volume at which the axisymmetric depression appears in the simulations, for different γ. Interpolating straight line: $\frac{\Delta V}{V} = 2.8\,\gamma^{-0.55}$. Secondary buckling: polygonization of the circular rim (black upward pointing triangles) and apparition of wrinkles (gray downward pointing triangles). Interpolating straight line: $\frac{\Delta V}{V} = 850\,\gamma^{-1}$.

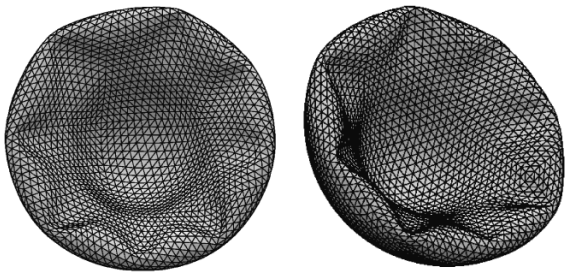

Fig. 11. Simulation with $\gamma = 15163$, $\nu = 0.333$ and $\frac{\Delta V}{V} = 0.645$. Such unusual conformation can be obtained from a capsule at lower γ; its energy is 1.42 times lower than the configuration with wrinkles ($W = 7$) obtained through progressive volume decrease for similar parameters.

one hemisphere within the other hemisphere, without an excessive cost in stretch energy.

It is interesting to note that a structure presenting 3 wrinkles had been obtained by Lim *et al.* [26] in simulations of red blood cells where the elastic properties of respectively the cytoskeleton and a homogeneous asymmetrical phospholipid bilayer were included in a similar numerical model with elastic bending, spontaneous curvature and stretching [40]. But the bending/stretching ratio in these biological objects, where bending and stretching have different origin, was higher than the range of similar values for a thin shell of isotropic material. This probably prevented these authors from obtaining shapes with more wrinkles.

Besides, the simulations presented here do not necessarily provide the energies of lowest configuration. As an example, we could, by following another path in the phase diagram of elastic and geometric parameters, obtain a totally new conformation of much lower energy than the wrinkled bowls (Fig. 11). But this conformation very likely corresponds to an energy trough too narrow to have been encountered in our experimental situation. Anyway, we are not looking for equilibrium configurations: we are trying to understand what really happens when a colloidal shell shrinks. It is well known that many buckling conformations can be quenched in non-absolute energy minima. Our study, putting into evidence qualitative as well as quantitative convergences between experiments, theory and simulations, strongly suggests that our simulations with a progressive decrease of the inner volume can reproduce the path followed by the buckling of real shells. The shapes observed are compatible both with self-contact, which would explain their stabilization, and with shell homogeneity. Besides, the conformation (and furthermore the number of wrinkles) gives an indication on the shell relative thickness range.

Structures comparable to wrinkled bowls have already been observed experimentally on millimetric half-spheres submitted to a localized [28,29] or a planar [41] load, theoretically forecasted [27,29], or numerically obtained by simulation of a sphere adhering on a flat surface [42], but here we did put in evidence that such structures can also be obtained with an isotropic force distribution.

6 Conclusion

Non-trivial buckled shapes were obtained by evaporating or dissolving the solvent enclosed in porous colloidal shells.

We have shown that the deformations of such objects are consistent with a model of homogeneous thin spherical shells with bending and in-plane stretching elasticity submitted to an isotropic external pressure. The numerical simulations showed that a primary buckling leading to capsules (holding a single axisymmetric depression) can be followed by a secondary buckling where the depression wrinkles. This happens for decreasing volume variations when the relative thickness of the shell is reduced, and the number of wrinkles concomitantly increases. Simulations and experiments qualitatively and quantitatively confirm each other.

These new results suggest that evaporation or dissolution of inner solvent is a promising way to obtain, from a monodisperse enough population of colloids, a monodisperse suspension of anisotropic objects with geometric parameters tunable through the characteristics of the initial spherical shell.

We thank L. Pauchard and N. Tsapis for their interest in this work, P. Peyla for elasticity discussions, S.J. Cox for his patient help in debugging SE subroutines, and K. Brakke for supplying and maintaining the free software Surface Evolver with impressive swiftness. This work was partially supported by the Deutsche Forschungsgemeinschaft (DFG) within the SFB-TR6 program "Physics of colloidal dispersions in external fields", and by the D. G. A. (Direction Générale de l'Armement).

References

1. A. Fernandez-Nieves, G. Cristobal, V. Garces-Chavez, G.C. Spalding, K. Dholakia, D.A. Weitz, Adv. Mater. **17**, 680 (2005).
2. I.O. Shklyarevskiy, P. Jonkheijm, P.C.M. Christianen, A.P.H.J. Shenning, E.W. Meijer, O. Henze, A.F.M. Kilbinger, W.J. Feast, A. Del Guerzo, J.-P. Desvergne, J.C. Maan, J. Am. Chem. Soc. **127**, 1112 (2005).
3. T. van Dillen, A. Polman, C.M. van Kats, A. van Blaaderen, Appl. Phys. Lett. **83**, 4315 (2003).
4. Y. Yin, Y. Lu, B. Gates, Y. Xia, J. Am. Chem. Soc. **123**, 8718 (2001).
5. V.N. Manoharan, M.T. Elsesser, D.J. Pine, Science **301**, 483 (2003).
6. P.M. Johnson, C.M. van Kats, A. van Blaaderen, Langmuir **21**, 11510 (2005).
7. D. Zerrouki, B. Rotenberg, S. Abramson *et al.*, Langmuir **22**, 57 (2006).
8. T. van Dillen, A. van Blaaderen, A. Polman, Mater. Today **7**, N. 7-8, 40 (2004).
9. C.M. Liddel, C.J. Summers, Adv. Mater. **15**, 1715 (2003).
10. N.C. Nanda, R. Schlief (Editors), in *Advances in Echo Imaging Using Contrast Enhancement* (Kluwer Academic Publishers, Dordrecht, 1993).
11. P. Marmottant, S. van der Meer, M. Emmer, M. Versluis, N. de Jong, S. Hilgenfeldt, D. Lohse, J. Acoustical Soc. Am. **118**, 3499 (2005).
12. O.I. Vinogradova, J. Phys.: Condens. Matter **16**, R1105 (2004).
13. S. Leporatti, A. Voigt, R. Mitlohner, G. Sukhorukov, E. Donath, H. Möhwald, Langmuir **16**, 4059 (2000).
14. F. Dubreuil, N. Elsner, A. Fery, Eur. Phys. J. E **12**, 215 (2003).
15. I.L. Ivanovska, P.J. de Pablo, B. Ibarra, G. Sgalari, F.C. MacKintosh, J.L. Carrasccosa, C.F. Schmidt, G.J.L. Wuite, Proc. Natl. Acad. Sci. U.S.A. **101**, 7600 (2004).
16. C. Gao, E. Donath, S. Moya, V. Dudnik, H. Möhwald, Eur. Phys. J. E **5**, 21 (2001).
17. J.P. Michel, I.L. Ivanovska, M.M. Gibbons, W.S. Klug, C.M. Knobler, G.J.L. Wuite, C.F. Schmidt, Proc. Natl. Acad. Sci. U.S.A. **103**, 6184 (2006).
18. A. Fery, R. Weinkamer, Polymer **48**, 7221 (2007).
19. C.I. Zoldesi, I.L. Ivanovska, G.J.L. Wuite, C. Quilliet, A. Imhof, in preparation.
20. C.I. Zoldesi, A. Imhof, Adv. Mater. **17**, 924 (2005).
21. C.I. Zoldesi, C.A. van Walree, A. Imhof, Langmuir **22**, 4343 (2006).
22. J. Ng Lee, C. Park, G.M. Whitesides, Anal. Chem. **75**, 6544 (2003).
23. M. Bessis, *Cytology of the Blood and Blood-Forming Organs* (Grune and Stratton, New York, 1956).
24. M. Okubo, H. Minami, K. Morikawa, Colloid Polym. Sci. **279**, 931 (2001).
25. M. Okubo, H. Minami, K. Morikawa, Colloid Polym. Sci. **281**, 214 (2003).
26. G.H.W. Lim, M. Wortis, R. Mukhopadhyay, Proc. Natl. Acad. Sci. U.S.A. **99**, 16766 (2002).
27. J.R. Fitch, Int. J. Solids Struct. **4**, 421 (1968).
28. L. Pauchard, S. Rica, Philos. Mag. B **78**, 225 (1998).
29. R. Kitching, R. Houlston, W. Johnson, Int. J. Mech. Sci. **17**, 693 (1975).
30. M. Ben Amar, Y. Pomeau, Proc. R. Soc. London, Ser. A **253**, 729 (1997).
31. W. Helfrich, Z. Naturforsch. C **28**, 693 (1973).
32. L. Pauchard, Y. Pomeau, S. Rica, C. R. Acad. Sci. II B, **324**, 411 (1997).
33. L. Landau, E.M. Lifshitz, *Theory of Elasticity*, third edition (Elsevier, Butterworth-Heinemann, Oxford, 1986).
34. N. Tsapis, E.R. Dufresne, S.S. Sinha, C.S. Riera, J.W. Hutchinson, L. Mahadevan, D.A. Weitz, Phys. Rev. Lett. **94**, 018302 (2005).
35. C. Quilliet, Phys. Rev. E. **74**, 046608 (2006).
36. K. Brakke, Exp. Math. **1**, 141 (1992).
37. J. Ng Lee, C. Park, G.M. Whitesides, Anal. Chem. **75**, 6544 (2003).
38. S. Chaïeb, F. Melo, J.-C. Géminard, Phys. Rev. Lett. **80**, 2354 (1998).
39. See, *e.g.*, U. Seifert, Adv. Phys. **46**, 13 (1997).
40. R. Mukhopadhyay, G.H.W. Lim, M. Wortis, Biophys. J., **82**, 1756 (2002).
41. Z. Cui, G. Moltschaniwskyj, D. Bhattacharyya, Comp. Struct. **66**, 591 (2004).
42. S. Komura, K. Tamura, T. Kato, Eur. Phys. J. E **18**, 343 (2005).

Eur. Phys. J. E **32**, 419-420 (2010)
DOI 10.1140/epje/i2010-10633-0

THE EUROPEAN PHYSICAL JOURNAL E

Erratum

Erratum to: Anisotropic colloids through non-trivial buckling

C. Quilliet[1,2,a], C. Zoldesi[2], C. Riera[3], A. van Blaaderen[2], and A. Imhof[2]

[1] Laboratoire de Spectrométrie Physique, CNRS UMR 5588 and Université Joseph Fourier, 140 avenue de la Physique, 38402 Saint-Martin d'Hères Cedex, France
[2] Soft Condensed Matter, Debye Institute for Nanomaterials Science, Faculty of Science, Utrecht University, Princetonplein 5, 3584 CC Utrecht, The Netherlands
[3] DEAS, Harvard University, 29, Oxford Street, Cambridge MA 02138, USA

Original article: Eur. Phys. J. E **27**, 13 (2008) DOI: 10.1140/epje/i2007-10365-2

Received 2 July 2010
Published online: 7 August 2010

The initial article presents experimental results on thin colloidal shells under constraint, numerical simulations of deformed spherical surfaces and calculations that are to be done in order to make the link between the 2D parameters of the numerical simulations and the 3D experimental parameters. The erratum concerns this latter aspect.

First group of corrections. Some calculations were erroneous, due to a misinterpretation of ref. [33].

The two equations between (2) and (3) of our original article,

$$A = \frac{1+2\sigma}{(1+\sigma)^2} Ed$$

and

$$\nu = \frac{\sigma}{1+\sigma},$$

are to be replaced with the following two equations:

$$A = Ed$$

and

$$\nu = \sigma.$$

This can be simply shown by writing Hooke's law with negligible out-of-plane constraints (see, *e.g.*, appendix A of Marmottant *et al.*, submitted to J. Acoust. Soc. Am.). It leads, for eq. (3)

$$\gamma = 12\left(1-\nu^2\right)\left(\frac{R}{d}\right)^2.$$

Another consequence is that $\left[1-\frac{2\nu^2}{1-\nu}\right]$ is to be replaced with $\left[1-\nu^2\right]$ in the equations between eq. (6) and eq. (7).

Second group of corrections. Mean curvature and related bending constant have diverging definitions between mathematicians/mechanicians on the one side, and the soft matter community (physics of vesicles) on the other side, which imposes to be very clear about which convention is used. Equation (1) was written in the soft matter convention, where mean curvature $c = \frac{1}{R_1} + \frac{1}{R_2}$ is the sum of the curvatures in the principal planes (and not the half-sum as considered by mathematicians). With this convention, the spontaneous curvature value effectively taken for the simulations was $c_0 = 2/R$ and not $1/R$ as written, which indeed corresponds to an initial constraint-free state.

[a] e-mail: Catherine.Quilliet@ujf-grenoble.fr

A similar confusion between the conventions of the two communities led to miscalculate the values of $\gamma = \frac{AR^2}{\kappa}$ effectively used in (still valid) simulations. All numerical values of γ displayed in our paper have thus to be multiplied by a factor 4.

As a consequence, the values of the corresponding tridimensional parameter $\frac{d}{R}$ displayed in text and captions have to be recalculated, using both the corrected equation (3) given in the previous paragraph of this erratum, and the corrected value of γ. All simulations having been performed at $\nu = 0.333$, corrections may be done by simply multiplying published values of $\frac{d}{R}$ by a factor $\frac{1}{\sqrt{3}} = 0.577$.

With these corrections, the two interpolating straight lines of fig. 10 have as equations: $\frac{\Delta V}{V} = 6\,\gamma^{-0.55}$ and $\frac{\Delta V}{V} = 3400\,\gamma^{-1}$, respectively, for the first-order and for the secondary buckling.